

LA-UR-19-32274 (Accepted Manuscript)

## Transport and Loss of Ring Current Electrons Inside Geosynchronous Orbit During the 17 March 2013 Storm

Aseev, N. A.  
Shprits, Y. Y.  
Wang, D.  
Drozdov, A. Y.  
Kellerman, A. C.  
Reeves, Geoffrey D.

Provided by the author(s) and the Los Alamos National Laboratory (2020-05-19).

**To be published in:** Journal of Geophysical Research: Space Physics

**DOI to publisher's version:** 10.1029/2018JA026031

**Permalink to record:** <http://permalink.lanl.gov/object/view?what=info:lanl-repo/lareport/LA-UR-19-32274>

**Disclaimer:**

Los Alamos National Laboratory, an affirmative action/equal opportunity employer, is operated by Triad National Security, LLC for the National Nuclear Security Administration of U.S. Department of Energy under contract 89233218CNA000001. By approving this article, the publisher recognizes that the U.S. Government retains nonexclusive, royalty-free license to publish or reproduce the published form of this contribution, or to allow others to do so, for U.S. Government purposes. Los Alamos National Laboratory requests that the publisher identify this article as work performed under the auspices of the U.S. Department of Energy. Los Alamos National Laboratory strongly supports academic freedom and a researcher's right to publish; as an institution, however, the Laboratory does not endorse the viewpoint of a publication or guarantee its technical correctness.

1                   **Explaining Transport of Ring Current Electrons Inside**  
2                   **Geosynchronous Orbit During 17 March 2013 storm**

3                   **N. A. Aseev<sup>1,2</sup>, Y. Y. Shprits<sup>1,2,3</sup>, D. Wang<sup>1</sup>, A. Y. Drozdov<sup>3</sup>, A. C. Kellerman<sup>3</sup>, G. D. Reeves<sup>4</sup>**

4   <sup>1</sup>GFZ German Research Centre for Geosciences, Potsdam, Germany

5   <sup>2</sup>Institute of Physics and Astronomy, University of Potsdam, Potsdam, Germany

6   <sup>3</sup>University of California Los Angeles, Los Angeles, CA, USA

7   <sup>4</sup>Los Alamos National Laboratory, Los Alamos, NM, USA

8                   **Key Points:**

- 9                   • We model ring current electron dynamics within GEO and estimate uncertainty  
10                    limits of the model
- 11                   • Van Allen Probe observations are within model uncertainty associated with bound-  
12                    ary conditions
- 13                   • Global electric and magnetic fields control ring current electron transport within  
14                    GEO

## 15 **Abstract**

16 The dynamics of ring current electrons (1-100 keV) plays an important role in the near-  
 17 Earth space weather. However, many questions regarding their major transport and loss  
 18 mechanisms are still open. In this study, we use the four-dimensional Versatile Electron  
 19 Radiation Belt code to model the enhancement of phase space density occurred during the  
 20 17 March 2013 storm. Our model includes ring current electron convection, radial diffu-  
 21 sion, and scattering into the Earth's atmosphere driven by whistler-mode hiss and chorus  
 22 waves. Our results show that electron transport from geostationary orbit to  $\sim 3.5 R_E$  is  
 23 driven by large-scale electric and magnetic fields. More accurate models of subauroral po-  
 24 larization streams and pitch-angle scattering may be required to explain the observations  
 25 below  $\sim 3.5 R_E$ . This study is the initial step towards understanding the dynamics of these  
 26 particles inside the geostationary orbit.

## 27 **1 Introduction**

28 The ring current electron population (energies from  $\sim 1$  to a few 100 keV) is an im-  
 29 portant driver of the near-Earth space weather. The electrons may provide from 10 to  
 30 25% of the ring current energy during storm times [*Frank, 1967; Liu et al., 2005; Zhao*  
 31 *et al., 2016*], therefore contributing significantly to equatorial disturbances of the Earth's  
 32 magnetic field. The injections of  $\sim 10$  keV electrons in the inner magnetosphere during  
 33 enhanced magnetospheric convection excite chorus waves [*Hwang et al., 2007; Thorne,*  
 34 *2010*] that resonate with relativistic electrons in the radiation belts and provide an effec-  
 35 tive mechanism of their pitch-angle scattering [*Horne and Thorne, 2003; Albert, 2005; Sh-*  
 36 *sprits et al., 2008; Thorne, 2010*] and local acceleration [*Horne and Thorne, 1998; Summers*  
 37 *et al., 1998; Horne et al., 2005; Li et al., 2007; Reeves et al., 2013*]. Electrons of 1-10 keV  
 38 energies can be deposited into protective shielding of satellites operating within the ring  
 39 current region, cause surface charging, and ultimately damage satellite electronics [*DeFor-*  
 40 *est, 1972; Baker, 2000; Choi et al., 2011; Thomsen et al., 2013; Ganushkina et al., 2017*].  
 41 Despite the important role of the ring current electrons, their transport and loss processes  
 42 within GEO remain poorly understood primarily due to the limited number of measure-  
 43 ments. Only several years ago Van Allen Probes have opened up a whole new opportunity  
 44 for quantitative tests of models and theory.

45 It still remains unclear which mechanisms are responsible for the earthward transport  
 46 of ring current electrons within GEO. It was suggested that the global dawn-dusk electric

47 field, driven by the dayside reconnection and antisunward magnetic field line convection,  
 48 together with corotation-driven radial electric field define electron drift path in the inner  
 49 magnetosphere [Kivelson and Southwood, 1975; Walker and Kivelson, 1975; Lyons and  
 50 Williams, 1984]. Supporting this theory, Korth *et al.* [1999] found that lines demarcating  
 51 enhanced electron flux at GEO match the Alfvén boundaries (the boundaries between open  
 52 and closed drift trajectories) calculated using Volland-Stern global electric field model  
 53 [Volland, 1973; Stern, 1975]. Using Polar data, Friedel *et al.* [2001] showed that electrons  
 54 are organized by the Alfvén boundaries within GEO, shrinking and allowing deeper access  
 55 of plasma during storm times.

56 It was proposed that energetic electrons can be injected in the magnetotail during  
 57 geomagnetically active times by substorm-related localized bursty bulk flows (BBFs) [An-  
 58 gelopoulos *et al.*, 1992, 1994; Runov *et al.*, 2009, 2011]. Gabrielse *et al.* [2012] showed  
 59 that the injections are driven by narrow channels of enhanced electric field associated with  
 60 the BBFs. However, the efficiency of this transport mechanism to inject particles inside  
 61 GEO has to be further investigated. DUBYAGIN *et al.* [2011] found that a significant fraction  
 62 of flow bursts is unable to penetrate within  $9 R_E$ , and OHTANI *et al.* [2006] concluded that  
 63 only a small portion of BBFs can reach geostationary distances. Further studies [Sergeev  
 64 *et al.*, 2012; Liu *et al.*, 2016] established that many BBFs are not accompanied by particle  
 65 injections. Liu *et al.* [2016] showed that only 20 of 71 events of dipolarization fronts de-  
 66 tected within GEO between 1 November 2012 and 1 November 2013 were associated with  
 67 energetic electron injections, typically not propagating closer than  $\sim 6 R_E$ .

68 An increase in large-scale electric fields between  $L = 3$  and  $L = 6$ , where  $L$  is McIl-  
 69 wain L-shell, for moderate to active geomagnetic conditions ( $K_p > 3$ ) was reported by  
 70 Rowland and Wygant [1998]. They showed that during the strongest geomagnetic activity  
 71 the enhanced electric fields can be observed inside  $L = 3$ . Later their results were con-  
 72 firmed by Califf *et al.* [2014]. The enhancement was attributed to subauroral polarization  
 73 streams (SAPS) [e.g. Foster and Burke, 2002; Foster and Vo, 2002], northward middle-  
 74 latitude ionospheric electric fields that arise from the separation between earthward ion  
 75 and electron plasma sheet boundaries [Southwood and Wolf, 1978] and usually pronounced  
 76 in the evening sector. Yet initial steps were made in order to understand how SAPS af-  
 77 fect electrons in the inner magnetosphere [Su *et al.*, 2016; Califf *et al.*, 2017; Lejosne *et al.*,  
 78 2018], more comprehensive modeling studies including electron transport and loss pro-  
 79 cesses are required.

80 Understanding the dynamics of the ring current electron population is a challeng-  
 81 ing task since the electron distribution significantly depends not only on time and radial  
 82 coordinate, as it is for the radiation belts, but also on magnetic local time (MLT). Multi-  
 83 spacecraft measurements covering different MLT sectors are therefore required to observe  
 84 the electron population in its global evolution. However, measuring this electron popu-  
 85 lation is complicated by different external effects such as surface charging and contam-  
 86 ination by photoelectrons and penetrating radiation (see *Denton et al.* [2017] and refer-  
 87 ences therein). Numerical modeling helps us gain insight into the dynamics of ring cur-  
 88 rent electrons under the scarcity of satellite measurements. Modern ring current mod-  
 89 els include electron population along with positively charged ions. Among the widely  
 90 used models are the Rice Convection Model (RCM) [*Toffoletto et al.*, 2003; *Lemon et al.*,  
 91 2004; *Chen et al.*, 2015], Ring Current-Atmosphere interactions model (RAM) [*Jordanova*  
 92 *et al.*, 1996; *Jordanova and Miyoshi*, 2005; *Jordanova et al.*, 2016], Comprehensive Inner-  
 93 Magnetosphere Ionosphere (CIMI) model [*Fok et al.*, 1999, 2011, 2014], Inner Magneto-  
 94 sphere Particle Transport and Acceleration Model (IMPTAM) [*Ganushkina et al.*, 2013,  
 95 2014, 2015], and Hot Electron Ion Drift Integrator (HEIDI) [*Liemohn et al.*, 2001; *Ilie*  
 96 *et al.*, 2012]. Recently, *Shprits et al.* [2015] developed the four-dimensional Versatile Elec-  
 97 tron Radiation Belt (VERB-4D) code that simultaneously describes the dynamics of the  
 98 ring current and relativistic radiation belt electrons in the prescribed electric and magnetic  
 99 fields.

100 All models typically face similar challenges in describing the dynamics of ring cur-  
 101 rent electrons. The models require spatial boundary conditions which specify ring current  
 102 source population originating from the plasma sheet, and electron loss rates due to local  
 103 interaction with different plasma waves present in the inner magnetosphere. Some ring  
 104 current models use boundary conditions that are set up in the plasma sheet beyond  $\sim 9 R_E$ ,  
 105 using statistical plasma parameters in the magnetotail [e.g. *Tsyganenko and Mukai*, 2003;  
 106 *Dubyagin et al.*, 2016]. Describing electron population within GEO becomes then a com-  
 107 plicated task since uncertainties associated with these boundary conditions are high and  
 108 processes controlling electron loss and transport beyond GEO are still not well understood  
 109 and quantified. Another approach that minimizes such uncertainties is to use observations  
 110 at GEO, utilizing satellites operating in that region. However, interpolation between the  
 111 L-shells and MLT at which measurements are available introduces large errors. Statis-  
 112 tical models based on measurements [e.g. *Denton et al.*, 2015, 2016] can provide MLT-

113 dependent electron flux at approximately the same L-shell. One approach, that is utilized  
 114 in this study, is to perform ensemble modeling by using a variety of boundary conditions  
 115 based on a statistical model within given uncertainty levels.

116 In this study, we use the VERB-4D code to understand the mechanisms which con-  
 117 trol transport of ring current electrons within GEO during the 17 March 2013 storm. In  
 118 Section 2, we present Van Allen Probe measurements of the storm. We describe the mod-  
 119 eling approach in Section 3. We show results in Section 4 and discuss them in Section 5.  
 120 Section 6 summarizes our findings.

## 121 2 Observations of the 17 March 2013 Storm

122 Figure 1a-c shows five-minute averaged electron phase space density (PSD) for the  
 123 first adiabatic invariant  $\mu = 0.1, 2.3,$  and  $9.9$  MeV/G and second invariant  $K = 0.3$   $G^{1/2}R_E$   
 124 computed using combined Van Allen Probe-B Helium, Oxygen, Proton, and Electron  
 125 (HOPE) Mass Spectrometer [Funsten *et al.*, 2013] and Magnetic Electron Ion Spectrom-  
 126 eter (MagEIS) [Blake *et al.*, 2013] observations during 17 March 2013 geomagnetic storm.  
 127 The apogee of the satellite is located at  $\sim 1$  h MLT, and the inbound satellite pass traverses  
 128 the postmidnight and prenoon MLT sectors while outbound pass crosses postnoon and  
 129 premidnight sectors. We used T04S [Tsyganenko and Sitnov, 2005] magnetic field model  
 130 incorporated into the IRBEM library [Boscher *et al.*, 2012] to calculate invariants  $\mu$  and  
 131  $K$  from observed local pitch angles and energies. To determine values of  $\mu$  we also uti-  
 132 lized magnetic field measurements made by Electric and Magnetic Field Instrument Suite  
 133 and Integrated Science (EMFISIS) [Kletzing *et al.*, 2013] aboard the satellite. Since val-  
 134 ues of  $\mu$  and  $K$  vary along the satellite trajectory, we used bilinear interpolation to calcu-  
 135 late PSD for given constant  $\mu$  and  $K$ . The chosen values of the invariants approximately  
 136 correspond to energies 0.3 keV, 9 keV, and 30 keV at GEO and 1 keV, 30 keV, and 100  
 137 keV at  $L=4$  (see Figure 2 illustrating energy and pitch angle dependence on the L-shell).  
 138 The corresponding pitch angles vary from  $\sim 34^\circ$  at GEO to  $40^\circ$  at  $L=3$ , which ensures that  
 139 Van Allen Probe data are available even if the satellite is significantly off the geomagnetic  
 140 equator that can happen during active times. Figure 1d shows the Kp and SYM-H indices.

141 The geomagnetic storm that occurred on 17 March 2013 was driven by coronal mass  
 142 ejection that hit the Earth magnetosphere at 06:00 UT (see Lyons *et al.* [2016] for more  
 143 details). In response to the storm, the Kp-index (Figure 1d) showed values above 6- for

144 18 hours, and SYM-H index (Figure 1d) reached  $-130$  nT, indicating significant enhance-  
 145 ment of the ring current. Ring current electrons were injected down to  $R_0 = 2.5-3 R_E$ ,  
 146 showing the increase in the PSD until the main phase of the storm ended on  $\sim 18$  March  
 147 (see Figure 1a-c). We note that  $R_0$  denotes here the distance from the center of the Earth  
 148 to the point of the minimum magnetic field found along the field line at which the space-  
 149 craft resides (for this, we used *Olson and Pfitzer* [1977] and IGRF [*Thébault et al.*, 2015]  
 150 magnetic field models). The recovery phase were characterized by the sharp decrease in  
 151 0.1 and 2.3 MeV/G electron PSD and more gradual decrease in 9.9 MeV/G electron PSD.

152 Yet the storm-time dynamics of electrons for considered values of  $\mu$  and  $K$  may  
 153 look similar, it can be driven by different energy-dependent mechanisms. Particles with  
 154 half-drift period longer than the main phase of the storm have direct convective access  
 155 to the ring current region [*Lyons and Williams*, 1980]. The higher-energy particles have  
 156 shorter drift periods and more efficiently interact with electric field fluctuations which lead  
 157 to the inward displacement driven by radial diffusion [*Cornwall*, 1968; *Lyons and Schulz*,  
 158 1989]. *Lyons and Schulz* [1989] showed that particles with energies  $\gtrsim 40$  keV are closer to  
 159 diffusive access while  $\lesssim 40$  keV particles have convective access.

### 160 3 Model Description

161 We use the VERB-4D code to model the dynamics of ring current electrons. The  
 162 code solves the modified Fokker-Planck equation with additional advection terms [*Shprits*  
 163 *et al.*, 2015; *Aseev et al.*, 2016]. It allows simultaneously modeling ring-current and radi-  
 164 ation belt dynamics by combining electron drift, radial diffusion, pitch-angle and energy  
 165 diffusion and loss processes that can be parameterized with the lifetime  $\tau$  (e.g. magne-  
 166 topause shadowing is accounted by setting up  $\tau$  to  $\frac{1}{2}$  drift period and loss to the atmo-  
 167 sphere is accounted by setting up the lifetimes within the loss cone to  $\frac{1}{4}$  bounce time):

$$\begin{aligned}
 \frac{\partial f}{\partial t} = & -\langle v_\varphi \rangle \frac{\partial f}{\partial \varphi} - \langle v_{R_0} \rangle \frac{\partial f}{\partial R_0} + \frac{1}{G} \frac{\partial}{\partial L^*} G \langle D_{L^*L^*} \rangle \frac{\partial f}{\partial L^*} + \\
 & + \frac{1}{G} \frac{\partial}{\partial V} G \left( \langle D_{VV} \rangle \frac{\partial f}{\partial V} + \langle D_{VK} \rangle \frac{\partial f}{\partial K} \right) + \frac{1}{G} \frac{\partial}{\partial K} G \left( \langle D_{KV} \rangle \frac{\partial f}{\partial V} + \langle D_{KK} \rangle \frac{\partial f}{\partial K} \right) - \frac{f}{\tau},
 \end{aligned} \tag{1}$$

168 where  $f$  is the PSD,  $t$  represents time,  $\varphi$  is MLT,  $R_0$  is the radial distance to a given point  
 169 in the geomagnetic equator,  $V$ ,  $K$  and  $L^*$  are modified adiabatic invariants [*Subbotin and*  
 170 *Shprits*, 2012],  $\tau$  is electron lifetime related to scattering into the loss cone and magne-  
 171 topause shadowing,  $\langle v_\varphi \rangle$  and  $\langle v_{R_0} \rangle$  are bounce-averaged drift velocities,  $\langle D_{L^*L^*} \rangle$ ,  $\langle D_{VV} \rangle$ ,  
 172  $\langle D_{VK} \rangle$ ,  $\langle D_{KV} \rangle$  and  $\langle D_{KK} \rangle$  are bounce-averaged diffusion coefficients,  $G = -2\pi B_0 R_E^2 \sqrt{8m_0 V} / (K +$

173  $0.5)^3/L^{*2}$  is the Jacobian of coordinate transformation from adiabatic invariants  $(\mu, J, \Phi)$   
 174 to  $(V, K, L^*)$  [Subbotin and Shprits, 2012],  $B_0$  is the field at the equator at the Earth's sur-  
 175 face,  $m_0$  is electron rest mass.

176 The spatial boundaries are set up at  $R_0 = 1$  and  $6.6 R_E$ , with  $0.5$  h and  $0.2 R_E$  grid  
 177 steps in MLT and radial distance, respectively. To construct a grid in  $V$  and  $K$ , we create  
 178 a logarithmic grid in energy and pitch angles limited by  $200$  eV and  $30$  keV and  $0.7^\circ$  and  
 179  $89.3^\circ$  at GEO with  $60$  nodes in energy and  $61$  nodes in pitch angle. Adiabatic invariants  
 180 are then calculated on this grid, using the dipole field model. We choose these energy  
 181 limits at GEO to fit in the statistical boundary condition model described below.

182 To model the enhancement of PSD during the main phase of the storm, we set up  
 183 initial conditions from Van Allen Probe-B inbound pass started at  $\sim 20 : 00$  UT 16 March  
 184 and ended at midnight on 17 March. We use PSD derived from HOPE and MagEIS mea-  
 185 surements, assume symmetry in MLT, and assign the calculated initial conditions to  $20 :$   
 186  $00$  UT 16 March. Boundary conditions in MLT are periodic. At the lower boundary  $R_0$   
 187  $= 1 R_E$ , we assume zero PSD since all particles are lost to the atmosphere. To specify  
 188 the outer boundary at  $R_0 = 6.6$ , we use the statistical model of electron fluxes developed  
 189 by Denton *et al.* [2016]. The model is based on 82 satellite-years of observations at GEO  
 190 made by magnetospheric plasma analyzer instruments onboard Los Alamos National Lab-  
 191 oratory satellites. The model provides spin-averaged electron fluxes as a function of en-  
 192 ergy, MLT and the Kp index and covers energy range from  $\sim 40$  eV to  $40$  keV at GEO.  
 193 Along with the mean and median values of the fluxes, 5th, 25th, 75th, and 95th percentile  
 194 limits are also given. To obtain directional flux from the spin-averaged flux, we assume its  
 195 sinusoidal dependence on the pitch angle.

196 We take into account electron scattering driven by hiss and chorus waves by using  
 197 parameterized electron lifetimes included in the parameter  $\tau$  instead of local diffusion  
 198 terms (fourth and fifth terms on the right-hand side of equation (1)). In this case, bound-  
 199 ary conditions in the invariants  $V$  and  $K$  are not required since there is no feedback from  
 200 local diffusion terms. We use the MLT-averaged model of electron lifetimes within the  
 201 plasmasphere developed by Orlova *et al.* [2016]. Outside the plasmasphere, we utilize the  
 202 MLT-dependent scattering rates obtained by [Gu *et al.*, 2012]. The plasmopause location is  
 203 calculated, using Carpenter and Anderson [1992] model.

204 We use realistic *Tsyganenko* [1989] (T89) magnetic field model and *Weimer* [2005]  
 205 (W05) polar cap potential model to calculate electron  $E \times B$  and gradient-curvature drift  
 206 velocities at the geomagnetic equator. The polar cap potential is mapped along the equipoten-  
 207 tial dipole field lines down to the geomagnetic equator. At the equator, the electric  
 208 field is numerically calculated, using central differencing scheme. Compared to commonly  
 209 used Kp-driven Volland-Stern electric field model, W05 model is parameterized with solar  
 210 wind parameters that ensures more realistic variability of the global electric field, naturally  
 211 driven by the dayside reconnection. In the current work, we feed 15-minute averaged solar  
 212 wind parameters to the W05 model.

213 We utilize Kp-parameterized radial diffusion rates by *Brautigam and Albert* [2000].  
 214 We note that similar results are obtained with *Ozeke et al.* [2014] parameterization. To  
 215 simultaneously account for the direct convective access and diffusive access of electrons  
 216 to the ring current region, we smoothly zero out the diffusion rates for electron energies  
 217 smaller than the threshold of 40 keV proposed by *Lyons and Schulz* [1989].

## 218 4 Results

219 We begin the simulation at 20:00 UT on 16 March 2013 with a time step of 15 min-  
 220 utes. We stop the simulation at 00:00 UT on 18 March 2013 to model the storm-time en-  
 221 hancement of PSD across the given range of energies. We then interpolate the global dis-  
 222 tribution of PSD provided by the VERB-4D code along the Van Allen Probe-B trajectory,  
 223 using linear interpolation in time, radial distance, and MLT. The target values of  $\mu$  and  
 224 K invariants to compare with satellite data were chosen to match the corresponding grid  
 225 values of the VERB-4D code.

226 Figure 3 shows the comparison between the Van Allen Probe-B data and our results  
 227 for  $\mu = 0.1, 2.3, \text{ and } 9.9 \text{ MeV/G}$  and  $K = 0.3 \text{ G}^{1/2} R_E$  for the outer radial boundary con-  
 228 ditions computed using the mean value of *Denton et al.* [2015] statistical flux distribution.  
 229 Each color-coded column corresponds to one satellite pass, and the left edge of the column  
 230 corresponds to the time of the beginning of the pass. The results for the first two satellite  
 231 passes, which started at 20:00 UT on 16 March and 00:00 UT on 17 March, remember  
 232 the information from initial conditions obtained from the data, thus approximately match-  
 233 ing the measurements. The storm-time enhancement of PSD along the next satellite pass  
 234 is generally reproduced in the model down to  $R_0 = \sim 3.5 R_E$  for all considered adiabatic

235 invariants. For this satellite pass, the VERB-4D results below  $R_0 = 3.5 R_E$  show PSD  
 236 values lower than observations below  $R_0 = 3.5 R_E$  for  $\mu = 0.1$  MeV/G and higher values  
 237 for  $\mu = 2.3$  MeV/G. The results for the subsequent modeled satellite passes approximately  
 238 match the observed radial extent of the ring current electron PSD for all considered adi-  
 239 abatic invariants. The modeled PSD profiles for  $\mu = 0.1$  MeV/G agree rather well with  
 240 the Van Allen Probe-B observations. The enhancements of electron PSD occur at similar  
 241 times as seen in data. The inner extent of the PSD profiles and the magnitude of the en-  
 242 hancements are also similar. The PSD profiles for  $\mu = 2.3$  MeV/G electrons approximately  
 243 match the radial structure of the measurements above  $R_0 = 4 R_E$  and show overestimation  
 244 near the inner edge between 3 and 4  $R_E$ . The increase in  $\mu = 9.9$  MeV/G PSD profiles  
 245 is also reproduced with the PSD values generally slightly lower than the observed values.  
 246 Comparison of the VERB-4D code results with the Van Allen Probe-A data is shown in  
 247 Supplementary Figure 1. Both satellites show similar evolution of electron PSD and the  
 248 code results interpolated along their trajectories have similar features (compare Figure 3  
 249 and Supplementary Figure 1).

250 To study the sensitivity of the simulation to the boundary conditions and provide ap-  
 251 proximate confidence interval of the model, we also perform simulations with 5th, 25th,  
 252 75th, and 95th percentiles of statistical distribution of electron flux at GEO [Denton *et al.*,  
 253 2015]. Figure 4 presents PSD profiles for  $\mu = 0.1, 2.3,$  and  $9.9$  MeV/G and  $K = 0.3 G^{1/2} R_E$   
 254 together with percentile limits for three subsequent satellite passes starting at 09:00 on  
 255 17 March. The figure shows that most of the time satellite data are within the percentile  
 256 limits, generally showing better agreement above  $R_0 = 3.5 R_E$  across all adiabatic invari-  
 257 ants. Note that PSD varies by up to 4 orders of magnitude and the model covers rather  
 258 well this variability within the confidence interval. Below  $3.5 R_E$   $\mu = 0.1$  MeV/G electron  
 259 PSD profiles diverge from simulation results, demonstrating deeper earthward displace-  
 260 ment by approximately  $0.3 R_E$  for the satellite pass that started at 09:00 (Figure 3a) and  
 261 lower PSD values for the next pass (Figure 3b), underestimating the inner boundary by ap-  
 262 proximately  $0.3 R_E$ . The results for 2.3 MeV/G are generally higher than the data for the  
 263 first two presented satellite passes between 3 and 4  $R_E$ , yet the satellite observations show  
 264 much better agreement at others radial distances. The values and shapes of PSD profiles  
 265 for  $\mu = 9.9$  MeV/G are very close to the 25th and 75th percentile limits across all radial  
 266 distances. Supplementary Figure 2 shows the comparison between data and the results for  
 267 mean boundary conditions, 5th and 95th percentiles for the whole modeled period.

## 5 Discussion

Generally good agreement between magnitude and shape of the modeled PSD profiles and Van Allen Probe observations for  $\mu = 0.1, 2.3,$  and  $9.9$  MeV/G electrons within GEO indicates that the storm-time transport of the particles down from GEO is primarily driven by the global-scale electric and magnetic fields and other mechanisms are not required to explain the general structure of electron transport from GEO to  $\sim 3.5 R_E$ . We note that  $0.1$  and  $2.3$  MeV/G electrons have direct convective access into the ring current region while  $9.9$  MeV/G particles have higher energies that require radial diffusion to reproduce the extent of the injections. Figure 5 shows that the inner boundary of the ring current electron distribution of  $9.9$  MeV/G electrons is significantly higher at the beginning of the storm for the simulation when radial diffusion is neglected while the results for  $\mu = 0.1$  and  $2.3$  MeV/G are the same for simulations with and without radial diffusion.

Ensemble simulations help us estimate model uncertainties related to boundary conditions. Figure 4 shows that the Van Allen Probe observations are almost all the time within the uncertainty limits above  $\sim 3.5 R_E$ . Results of the simulations driven by 75th and 95th percentiles of boundary condition fluxes mostly overestimate data above  $\sim 3.5 R_E$  which indicates that the agreement between the results and data is not achieved due to artificially included injections in the overestimated boundary conditions. Note that the model error of the simulation driven by the mean outer spatial boundary conditions is typically small between  $5$  and  $6 R_E$  (see Figure 4). This fact suggests that the bigger differences between simulation results below are not related to the transport from plasma sheet and can be driven by inaccuracies in loss or transport processes in the inner magnetosphere. We also note that the used percentile values provide estimates of confidence interval for boundary conditions since they also contain an uncertainty associated with the conversion from spin-averaged to directional flux. The confidence interval-type estimates are especially helpful in validating model results with data for low-energy particles because of their complicated MLT-dependent dynamics affected by a number of parameters (e.g. electron loss rates, electric and magnetic field models, and boundary conditions).

The discrepancy of the model and measurements below  $\sim 3.5 R_E$  can be explained by uncertainties in electron loss rates or by the fact that SAPS electric fields are not taken into account in the model. To estimate an effect of SAPS, we performed a simulation with the included Kp-dependent model of SAPS, using the approach developed by *Goldstein*

300 *et al.* [2005]. Figure 6 shows the results in the same format as Figure 4. The overall effect  
 301 of the SAPS is not pronounced:  $\mu = 0.1$  MeV/G PSD profiles show stronger underestima-  
 302 tion around  $3.5 R_E$  at 13:30 UT, and  $\mu = 2.3$  MeV/G are propagated slightly closer to the  
 303 Earth.

304 One potential reason for the difference between our model and data is inaccuracies  
 305 in the electron loss parameterization. To more accurately model pitch angle scattering,  
 306 utilizing local diffusion coefficients calculated using MLT-dependent wave models is re-  
 307 quired. Currently such models for chorus waves are not available, and they need to be  
 308 developed in the future. We also note the importance of the plasmasphere model that sep-  
 309 arates hiss and chorus wave-driven scattering of electrons. Uncertainty in the demarcation  
 310 boundary between the regions dominated by different wave models and different plasma  
 311 conditions introduces additional uncertainty in the simulations. More advanced MLT-  
 312 dependent models (e.g. derived from neural network-based model of plasmasphere [e.g.  
 313 *Zhelavskaya et al.*, 2017]) will be included in our future studies.

## 314 **6 Summary**

315 In this study, we modeled storm-time enhancement of ring current electron PSD  
 316 during 17 March 2013 storm. Our model includes magnetospheric convection driven by  
 317 global magnetic and electric fields, radial diffusion, and electron scattering rates due to in-  
 318 teraction with whistler-mode hiss and chorus waves. Our results showed that global mag-  
 319 netic and electric fields control the earthward transport of the electrons, and additional  
 320 mechanisms are not required to explain the general dynamics of the electrons from GEO  
 321 into the ring current region. We note that additional mechanisms such as dipolarization  
 322 fronts, double layers, and other types of localized electric field-induced transport may turn  
 323 out to be dominant beyond GEO. These mechanisms may also potentially contribute to  
 324 injections inside GEO but will not dominate over convective transport and wave-induced  
 325 loss. We demonstrated that the Van Allen Probe data are mostly within the uncertainties  
 326 associated with the outer radial boundary conditions above  $3.5 R_E$ . The discrepancies of  
 327 the VERB-4D results and data below  $3.5 R_E$  may be associated with the inaccuracies of  
 328 the electron lifetime model or with the neglect of SAPS electric fields. We tested simplest  
 329 SAPS model [*Goldstein et al.*, 2005] but its effect on the considered electron energy range  
 330 did not appear to be significant. This study presents the initial step towards understanding  
 331 the complicated transport and loss processes of low-energy electrons within GEO. The fu-

332     ture extension of this study will include modeling of lower energy electrons, improvement  
 333     of loss model, and understanding of the contribution of localized electric fields beyond  
 334     GEO.

### 335     **Acknowledgments**

336     The authors acknowledge use of NASA/GSFC's Space Physics Data Facility's OMNIWeb  
 337     service, and OMNI data. The Kp index was provided by GFZ Potsdam. The authors are  
 338     grateful to the RBSP-ECT team for the provision of Van Allen Probes observations. All  
 339     RBSP-ECT data are publicly available at the web site <http://www.RBSP-ect.lanl.gov/>. This  
 340     research was supported by the Helmholtz-Gemeinschaft (HGF) [10.13039/501100001656],  
 341     NASA grants NNX15AI94G and NNX16AG78G, NSF grant AGS-1552321, and project  
 342     PROGRESS funded by EC | Horizon 2020 Framework Programme (H2020) [10.13039/100010661]  
 343     (637302)). The research has been partially funded by Deutsche Forschungsgemeinschaft  
 344     (DFG) through grant CRC 1294 Data Assimilation, Project B06. Processing and analysis  
 345     of the ECT data was supported by Energetic Particle, Composition, and Thermal Plasma  
 346     (RBSP-ECT) investigation funded under NASA's Prime contract no. NAS5-01072. This  
 347     work used computational and storage services associated with the Hoffman2 Shared Clus-  
 348     ter provided by UCLA Institute for Digital Research and Education's Research Technology  
 349     Group. The authors thank the developers of the IRBEM library which was adapted for use  
 350     in the current study and Daniel Weimer for the provision of the codes for global electric  
 351     field model. The authors thank Irina Zhelavskaya and Frederic Effenberger for useful dis-  
 352     cussions.

### 353     **References**

- 354     Albert, J. M. (2005), Evaluation of quasi-linear diffusion coefficients for whistler mode  
 355     waves in a plasma with arbitrary density ratio, *Journal of Geophysical Research: Space*  
 356     *Physics*, *110*(A3), doi:10.1029/2004JA010844.
- 357     Angelopoulos, V., W. Baumjohann, C. F. Kennel, F. V. Coroniti, M. G. Kivelson, R. Pel-  
 358     lat, R. J. Walker, H. Lühr, and G. Paschmann (1992), Bursty bulk flows in the inner  
 359     central plasma sheet, *Journal of Geophysical Research: Space Physics*, *97*(A4), 4027–  
 360     4039, doi:10.1029/91JA02701.
- 361     Angelopoulos, V., C. F. Kennel, F. V. Coroniti, R. Pellat, M. G. Kivelson, R. J. Walker,  
 362     C. T. Russell, W. Baumjohann, W. C. Feldman, and J. T. Gosling (1994), Statistical

- 363 characteristics of bursty bulk flow events, *Journal of Geophysical Research: Space*  
 364 *Physics*, 99(A11), 21,257–21,280, doi:10.1029/94JA01263.
- 365 Aseev, N. A., Y. Y. Shprits, A. Y. Drozdov, and A. C. Kellerman (2016), Numerical ap-  
 366 plications of the advective-diffusive codes for the inner magnetosphere, *Space Weather*,  
 367 14(11), 993–1010, doi:10.1002/2016SW001484.
- 368 Baker, D. N. (2000), The occurrence of operational anomalies in spacecraft and their re-  
 369 lationship to space weather, *IEEE Transactions on Plasma Science*, 28(6), 2007–2016,  
 370 doi:10.1109/27.902228.
- 371 Blake, J. B., P. A. Carranza, S. G. Claudepierre, J. H. Clemmons, W. R. Crain, Y. Dotan,  
 372 J. F. Fennell, F. H. Fuentes, R. M. Galvan, J. S. George, et al. (2013), The magnetic  
 373 electron ion spectrometer (mageis) instruments aboard the radiation belt storm probes  
 374 (RBSP) spacecraft, *Space Science Reviews*, 179(1-4), 383–421, doi:10.1007/s11214-013-  
 375 9991-8.
- 376 Boscher, D., S. Bourdarie, P. O'Brien, and T. Guild (2012), Irbem-lib library  
 377 (<http://irbem.sourceforge.net>).
- 378 Brautigam, D. H., and J. M. Albert (2000), Radial diffusion analysis of outer radiation belt  
 379 electrons during the October 9, 1990, magnetic storm, *Journal of Geophysical Research:*  
 380 *Space Physics*, 105(A1), 291–309, doi:10.1029/1999JA900344.
- 381 Califf, S., X. Li, L. Blum, A. Jaynes, Q. Schiller, H. Zhao, D. Malaspina, M. Hartinger,  
 382 R. A. Wolf, D. E. Rowland, et al. (2014), THEMIS measurements of quasi-static elec-  
 383 tric fields in the inner magnetosphere, *Journal of Geophysical Research: Space Physics*,  
 384 119(12), 9939–9951, doi:10.1002/2014JA020360.
- 385 Califf, S., X. Li, H. Zhao, A. Kellerman, T. E. Sarris, A. Jaynes, and D. M. Malaspina  
 386 (2017), The role of the convection electric field in filling the slot region between the  
 387 inner and outer radiation belts, *Journal of Geophysical Research: Space Physics*, 122(2),  
 388 2051–2068, doi:10.1002/2016JA023657.
- 389 Carpenter, D. L., and R. R. Anderson (1992), An ISEE/whistler model of equatorial elec-  
 390 tron density in the magnetosphere, *Journal of Geophysical Research: Space Physics*,  
 391 97(A2), 1097–1108, doi:10.1029/91JA01548.
- 392 Chen, M. W., C. L. Lemon, K. Orlova, Y. Shprits, J. Hecht, and R. L. Walterscheid  
 393 (2015), Comparison of simulated and observed trapped and precipitating electron fluxes  
 394 during a magnetic storm, *Geophysical Research Letters*, 42(20), 8302–8311.

- 395 Choi, H.-S., J. Lee, K.-S. Cho, Y.-S. Kwak, I.-H. Cho, Y.-D. Park, Y.-H. Kim, D. N.  
 396 Baker, G. D. Reeves, and D.-K. Lee (2011), Analysis of GEO spacecraft anomalies:  
 397 Space weather relationships, *Space Weather*, 9(6), doi:10.1029/2010SW000597.
- 398 Cornwall, J. M. (1968), Diffusion processes influenced by conjugate-point wave phenom-  
 399 ena, *Radio science*, 3(7), 740–744, doi:10.1002/rds196837740.
- 400 DeForest, S. E. (1972), Spacecraft charging at synchronous orbit, *Journal of Geophysical*  
 401 *Research*, 77(4), 651–659, doi:10.1029/JA077i004p00651.
- 402 Denton, M. H., M. F. Thomsen, V. K. Jordanova, M. G. Henderson, J. E. Borovsky, J. S.  
 403 Denton, D. Pitchford, and D. P. Hartley (2015), An empirical model of electron and ion  
 404 fluxes derived from observations at geosynchronous orbit, *Space Weather*, 13(4), 233–  
 405 249, doi:10.1002/2015SW001168.
- 406 Denton, M. H., M. G. Henderson, V. K. Jordanova, M. F. Thomsen, J. E. Borovsky,  
 407 J. Woodroffe, D. P. Hartley, and D. Pitchford (2016), An improved empirical model of  
 408 electron and ion fluxes at geosynchronous orbit based on upstream solar wind condi-  
 409 tions, *Space Weather*, 14(7), 511–523, doi:10.1002/2016SW001409.
- 410 Denton, M. H., G. D. Reeves, B. A. Larsen, R. F. W. Friedel, M. F. Thomsen, P. A.  
 411 Fernandes, R. M. Skoug, H. O. Funsten, and L. K. Sarno-Smith (2017), On the ori-  
 412 gin of low-energy electrons in the inner magnetosphere: Fluxes and pitch-angle dis-  
 413 tributions, *Journal of Geophysical Research: Space Physics*, 122(2), 1789–1802, doi:  
 414 10.1002/2016JA023648.
- 415 Dubyagin, S., V. Sergeev, S. Apatenkov, V. Angelopoulos, A. Runov, R. Nakamura,  
 416 W. Baumjohann, J. McFadden, and D. Larson (2011), Can flow bursts penetrate into the  
 417 inner magnetosphere?, *Geophysical Research Letters*, 38(8), doi:10.1029/2011GL047016.
- 418 Dubyagin, S., N. Y. Ganushkina, I. Sillanpää, and A. Runov (2016), Solar wind-driven  
 419 variations of electron plasma sheet densities and temperatures beyond geostationary or-  
 420 bit during storm times, *Journal of Geophysical Research: Space Physics*, 121(9), 8343–  
 421 8360, doi:10.1002/2016JA022947.
- 422 Fok, M.-C., T. E. Moore, and D. C. Delcourt (1999), Modeling of inner plasma sheet  
 423 and ring current during substorms, *Journal of Geophysical Research: Space Physics*,  
 424 104(A7), 14,557–14,569, doi:10.1029/1999JA900014.
- 425 Fok, M.-C., A. Glocer, Q. Zheng, R. B. Horne, N. P. Meredith, J. M. Albert, and  
 426 T. Nagai (2011), Recent developments in the radiation belt environment model,  
 427 *Journal of Atmospheric and Solar-Terrestrial Physics*, 73(11-12), 1435–1443, doi:

- 428 10.1016/j.jastp.2010.09.033.
- 429 Fok, M.-C., N. Y. Buzulukova, S.-H. Chen, A. Glocer, T. Nagai, P. Valek, and J. Perez  
430 (2014), The Comprehensive Inner Magnetosphere-Ionosphere Model, *Journal of Geo-*  
431 *physical Research: Space Physics*, 119(9), 7522–7540, doi:10.1002/2014JA020239.
- 432 Foster, J. C., and W. J. Burke (2002), SAPS: A new categorization for sub-auroral elec-  
433 tric fields, *Eos, Transactions American Geophysical Union*, 83(36), 393–394, doi:  
434 10.1029/2002EO000289.
- 435 Foster, J. C., and H. B. Vo (2002), Average characteristics and activity dependence of  
436 the subauroral polarization stream, *Journal of Geophysical Research: Space Physics*,  
437 107(A12), doi:10.1029/2002JA009409.
- 438 Frank, L. A. (1967), Several observations of low-energy protons and electrons in the  
439 Earth's magnetosphere with OGO 3, *Journal of Geophysical Research*, 72(7), 1905–  
440 1916, doi:10.1029/JZ072i007p01905.
- 441 Friedel, R. H. W., H. Korth, M. G. Henderson, M. F. Thomsen, and J. D. Scudder (2001),  
442 Plasma sheet access to the inner magnetosphere, *Journal of Geophysical Research:*  
443 *Space Physics*, 106(A4), 5845–5858, doi:10.1029/2000JA003011.
- 444 Funsten, H. O., R. M. Skoug, A. A. Guthrie, E. A. MacDonald, J. R. Baldonado, R. W.  
445 Harper, K. C. Henderson, K. H. Kihara, J. E. Lake, B. A. Larsen, et al. (2013), Helium,  
446 Oxygen, Proton, and Electron (HOPE) mass spectrometer for the radiation belt storm  
447 probes mission, *Space Science Reviews*, 179(1-4), 423–484, doi:10.1007/s11214-013-  
448 9968-7.
- 449 Gabrielse, C., V. Angelopoulos, A. Runov, and D. L. Turner (2012), The effects of tran-  
450 sient, localized electric fields on equatorial electron acceleration and transport toward  
451 the inner magnetosphere, *Journal of Geophysical Research: Space Physics*, 117(A10),  
452 doi:doi.org/10.1029/2012JA017873.
- 453 Ganushkina, N., A. Jaynes, and M. Liemohn (2017), Space weather effects produced  
454 by the ring current particles, *Space Science Reviews*, 212(3-4), 1315–1344, doi:  
455 10.1007/s11214-017-0412-2.
- 456 Ganushkina, N. Y., O. A. Amariutei, Y. Y. Shprits, and M. W. Liemohn (2013), Transport  
457 of the plasma sheet electrons to the geostationary distances, *Journal of Geophysical Re-*  
458 *search: Space Physics*, 118(1), 82–98, doi:10.1029/2012JA017923.
- 459 Ganushkina, N. Y., M. W. Liemohn, O. A. Amariutei, and D. Pitchford (2014), Low-  
460 energy electrons (5–50 keV) in the inner magnetosphere, *Journal of Geophysical Re-*

- 461 *search: Space Physics, 119(1), 246–259, doi:10.1002/2013JA019304.*
- 462 Ganushkina, N. Y., O. A. Amariutei, D. Welling, and D. Heynderickx (2015), Nowcast  
463 model for low-energy electrons in the inner magnetosphere, *Space Weather, 13(1), 16–*  
464 *34, doi:10.1002/2014SW001098.*
- 465 Goldstein, J., J. L. Burch, and B. R. Sandel (2005), Magnetospheric model of subauro-  
466 ral polarization stream, *Journal of Geophysical Research: Space Physics, 110(A9), doi:*  
467 *10.1029/2005JA011135.*
- 468 Gu, X., Y. Y. Shprits, and B. Ni (2012), Parameterized lifetime of radiation belt electrons  
469 interacting with lower-band and upper-band oblique chorus waves, *Geophysical Research*  
470 *Letters, 39(15), doi:10.1029/2012GL052519.*
- 471 Horne, R. B., and R. M. Thorne (1998), Potential waves for relativistic electron scatter-  
472 ing and stochastic acceleration during magnetic storms, *Geophysical Research Letters,*  
473 *25(15), 3011–3014, doi:10.1029/98GL01002.*
- 474 Horne, R. B., and R. M. Thorne (2003), Relativistic electron acceleration and precipitation  
475 during resonant interactions with whistler-mode chorus, *Geophysical research letters,*  
476 *30(10), doi:10.1029/2003GL016973.*
- 477 Horne, R. B., R. M. Thorne, Y. Y. Shprits, N. P. Meredith, S. A. Glauert, A. J. Smith,  
478 S. G. Kanekal, D. N. Baker, M. J. Engebretson, J. L. Posch, et al. (2005), Wave ac-  
479 celeration of electrons in the Van Allen radiation belts, *Nature, 437(7056), 227, doi:*  
480 *10.1038/nature03939.*
- 481 Hwang, J.-A., D.-Y. Lee, L. R. Lyons, A. J. Smith, S. Zou, K. W. Min, K.-H. Kim, Y.-J.  
482 Moon, and Y. Park (2007), Statistical significance of association between whistler-mode  
483 chorus enhancements and enhanced convection periods during high-speed streams, *Jour-*  
484 *nal of Geophysical Research: Space Physics, 112(A9), doi:10.1029/2007JA012388.*
- 485 Ilie, R., M. W. Liemohn, G. Toth, and R. M. Skoug (2012), Kinetic model of the inner  
486 magnetosphere with arbitrary magnetic field, *Journal of Geophysical Research: Space*  
487 *Physics, 117(A4), doi:10.1029/2011JA017189.*
- 488 Jordanova, V. K., and Y. Miyoshi (2005), Relativistic model of ring current and radia-  
489 tion belt ions and electrons: Initial results, *Geophysical research letters, 32(14), doi:*  
490 *10.1029/2005GL023020.*
- 491 Jordanova, V. K., L. M. Kistler, J. U. Kozyra, G. V. Khazanov, and A. F. Nagy (1996),  
492 Collisional losses of ring current ions, *Journal of Geophysical Research: Space Physics,*  
493 *101(A1), 111–126, doi:10.1029/95JA02000.*

- 494 Jordanova, V. K., W. Tu, Y. Chen, S. K. Morley, A.-D. Panaitescu, G. D. Reeves, and  
495 C. A. Kletzing (2016), RAM-SCB simulations of electron transport and plasma wave  
496 scattering during the October 2012 "double-dip" storm, *Journal of Geophysical  
497 Research: Space Physics*, *121*(9), 8712–8727, doi:10.1002/2016JA022470.
- 498 Kivelson, M. G., and D. J. Southwood (1975), Approximations for the study of drift  
499 boundaries in the magnetosphere, *Journal of Geophysical Research*, *80*(25), 3528–3534,  
500 doi:10.1029/JA080i025p03528.
- 501 Kletzing, C. A., W. S. Kurth, M. Acuna, R. J. MacDowall, R. B. Torbert, T. Averkamp,  
502 D. Bodet, S. R. Bounds, M. Chutter, J. Connerney, et al. (2013), The electric and mag-  
503 netic field instrument suite and integrated science (EMFISIS) on RBSP, *Space Science  
504 Reviews*, *179*(1-4), 127–181, doi:10.1007/s11214-013-9993-6.
- 505 Korth, H., M. F. Thomsen, J. E. Borovsky, and D. J. McComas (1999), Plasma sheet  
506 access to geosynchronous orbit, *Journal of Geophysical Research: Space Physics*,  
507 *104*(A11), 25,047–25,061, doi:doi.org/10.1029/1999JA900292.
- 508 Lejosne, S., B. S. R. Kunduri, F. S. Mozer, and D. L. Turner (2018), Energetic Electron  
509 Injections Deep Into the Inner Magnetosphere: A Result of the Subauroral Polarization  
510 Stream (SAPS) Potential Drop, *Geophysical Research Letters*, *45*(9), 3811–3819.
- 511 Lemon, C., R. A. Wolf, T. W. Hill, S. Sazykin, R. W. Spiro, F. R. Toffoletto, J. Birn, and  
512 M. Hesse (2004), Magnetic storm ring current injection modeled with the Rice Con-  
513 vection Model and a self-consistent magnetic field, *Geophysical research letters*, *31*(21),  
514 doi:10.1029/2004GL020914.
- 515 Li, W., Y. Y. Shprits, and R. M. Thorne (2007), Dynamic evolution of energetic outer  
516 zone electrons due to wave-particle interactions during storms, *Journal of Geophysical  
517 Research: Space Physics*, *112*(A10), doi:10.1029/2007JA012368.
- 518 Liemohn, M. W., J. U. Kozyra, C. R. Clauer, and A. J. Ridley (2001), Computational  
519 analysis of the near-Earth magnetospheric current system during two-phase decay  
520 storms, *Journal of Geophysical Research: Space Physics*, *106*(A12), 29,531–29,542, doi:  
521 10.1029/2001JA000045.
- 522 Liu, J., V. Angelopoulos, X.-J. Zhang, D. L. Turner, C. Gabrielse, A. Runov, J. Li, H. O.  
523 Funsten, and H. E. Spence (2016), Dipolarizing flux bundles in the cis-geosynchronous  
524 magnetosphere: Relationship between electric fields and energetic particle injec-  
525 tions, *Journal of Geophysical Research: Space Physics*, *121*(2), 1362–1376, doi:  
526 10.1002/2015JA021691.

- 527 Liu, S., M. W. Chen, J. L. Roeder, L. R. Lyons, and M. Schulz (2005), Relative contri-  
 528 bution of electrons to the stormtime total ring current energy content, *Geophysical re-*  
 529 *search letters*, 32(3), doi:10.1029/2004GL021672.
- 530 Lyons, L. R., and M. Schulz (1989), Access of energetic particles to storm time ring cur-  
 531 rent through enhanced radial diffusion, *Journal of Geophysical Research: Space*  
 532 *Physics*, 94(A5), 5491–5496, doi:10.1029/JA094iA05p05491.
- 533 Lyons, L. R., and D. J. Williams (1980), A source for the geomagnetic storm main phase  
 534 ring current, *Journal of Geophysical Research: Space Physics*, 85(A2), 523–530, doi:  
 535 10.1029/JA085iA02p00523.
- 536 Lyons, L. R., and D. J. Williams (1984), *Quantitative aspects of magnetospheric physics*,  
 537 231 pp., D. Reidel Publishing Company, Dordrecht-Boston-Lancaster.
- 538 Lyons, L. R., B. Gallardo-Lacourt, S. Zou, J. M. Weygand, Y. Nishimura, W. Li,  
 539 M. Gkioulidou, V. Angelopoulos, E. F. Donovan, J. M. Ruohoniemi, et al. (2016),  
 540 The 17 March 2013 storm: Synergy of observations related to electric field modes and  
 541 their ionospheric and magnetospheric Effects, *Journal of Geophysical Research: Space*  
 542 *Physics*, 121(11), doi:10.1002/2016JA023237.
- 543 Ohtani, S., H. J. Singer, and T. Mukai (2006), Effects of the fast plasma sheet flow on the  
 544 geosynchronous magnetic configuration: Geotail and GOES coordinated study, *Journal*  
 545 *of Geophysical Research: Space Physics*, 111(A1), doi:10.1029/2005JA011383.
- 546 Olson, W. P., and K. A. Pfitzer (1977), Magnetospheric magnetic field modeling ann. sci.  
 547 rep, Contract F44620-75-C-0033, Air Force Off. of Sci. Res., McDonnell Douglas Astro-  
 548 nautics Co., Huntington Beach, Calif.
- 549 Orlova, K., Y. Shprits, and M. Spasojevic (2016), New global loss model of energetic and  
 550 relativistic electrons based on Van Allen Probes measurements, *Journal of Geophysical*  
 551 *Research: Space Physics*, 121(2), 1308–1314, doi:10.1002/2015JA021878.
- 552 Ozeke, L. G., I. R. Mann, K. R. Murphy, J. R. I., and D. K. Milling (2014), Analytic ex-  
 553 pressions for ULF wave radiation belt radial diffusion coefficients, *Journal of Geophys- ical*  
 554 *Research: Space Physics*, 119(3), 1587–1605, doi:10.1002/2013JA019204.
- 555 Reeves, G. D., H. E. Spence, M. G. Henderson, S. K. Morley, R. H. W. Friedel, H. O.  
 556 Funsten, D. N. Baker, S. G. Kanekal, J. B. Blake, J. F. Fennell, et al. (2013), Electron  
 557 acceleration in the heart of the Van Allen radiation belts, *Science*, 341(6149), 991–994,  
 558 doi:10.1126/science.1237743.

- 559 Rowland, D. E., and J. R. Wygant (1998), Dependence of the large-scale, inner magneto-  
560 spheric electric field on geomagnetic activity, *Journal of Geophysical Research: Space*  
561 *Physics*, *103*(A7), 14,959–14,964, doi:10.1029/97JA03524.
- 562 Runov, A., V. Angelopoulos, M. I. Sitnov, V. A. Sergeev, J. Bonnell, J. P. McFadden,  
563 D. Larson, K.-H. Glassmeier, and U. Auster (2009), THEMIS observations of an  
564 earthward-propagating dipolarization front, *Geophysical Research Letters*, *36*(14), doi:  
565 10.1029/2009GL038980.
- 566 Runov, A., V. Angelopoulos, X.-Z. Zhou, X.-J. Zhang, S. Li, F. Plaschke, and J. Bon-  
567 nell (2011), A THEMIS multicasestudy of dipolarization fronts in the magneto-  
568 tail plasma sheet, *Journal of Geophysical Research: Space Physics*, *116*(A5), doi:  
569 10.1029/2010JA016316.
- 570 Sergeev, V. A., I. A. Chernyaev, S. V. Dubyagin, Y. Miyashita, V. Angelopoulos, P. D.  
571 Boakes, R. Nakamura, and M. G. Henderson (2012), Energetic particle injections to  
572 geostationary orbit: Relationship to flow bursts and magnetospheric state, *Journal of*  
573 *Geophysical Research: Space Physics*, *117*(A10), doi:10.1029/2012JA017773.
- 574 Shprits, Y. Y., D. A. Subbotin, N. P. Meredith, and S. R. Elkington (2008), Review of  
575 modeling of losses and sources of relativistic electrons in the outer radiation belt II: Lo-  
576 cal acceleration and loss, *Journal of Atmospheric and Solar-Terrestrial Physics*, *70*(14),  
577 1694–1713, doi:10.1016/j.jastp.2008.06.014.
- 578 Shprits, Y. Y., A. C. Kellerman, A. Y. Drozdov, H. E. Spence, G. D. Reeves, and D. N.  
579 Baker (2015), Combined convective and diffusive simulations: VERB-4D compari-  
580 son with 17 March 2013 Van Allen Probes observations, *Geophysical Research Letters*,  
581 *42*(22), 9600–9608, doi:10.1002/2015GL065230.
- 582 Southwood, D. J., and R. A. Wolf (1978), An assessment of the role of precipitation in  
583 magnetospheric convection, *Journal of Geophysical Research: Space Physics*, *83*(A11),  
584 5227–5232, doi:10.1029/JA083iA11p05227.
- 585 Stern, D. P. (1975), The motion of a proton in the equatorial magnetosphere, *Journal of*  
586 *Geophysical Research*, *80*(4), 595–599, doi:10.1029/JA080i004p00595.
- 587 Su, Y.-J., R. S. Selesnick, and J. B. Blake (2016), Formation of the inner electron radia-  
588 tion belt by enhanced large-scale electric fields, *Journal of Geophysical Research: Space*  
589 *Physics*, *121*(9), 8508–8522, doi:10.1002/2016JA022881.
- 590 Subbotin, D. A., and Y. Y. Shprits (2012), Three-dimensional radiation belt simulations  
591 in terms of adiabatic invariants using a single numerical grid, *Journal of Geophysical*

- 592 *Research: Space Physics*, 117(A5), doi:10.1029/2011JA017467.
- 593 Summers, D., R. M. Thorne, and F. Xiao (1998), Relativistic theory of wave-particle reso-  
594 nant diffusion with application to electron acceleration in the magnetosphere, *Journal of*  
595 *Geophysical Research: Space Physics*, 103(A9), 20,487–20,500, doi:10.1029/98JA01740.
- 596 Thébault, E., C. C. Finlay, C. D. Beggan, P. Alken, J. Aubert, O. Barrois, F. Bertrand,  
597 T. Bondar, A. Boness, L. Brocco, et al. (2015), International geomagnetic reference  
598 field: the 12th generation, *Earth, Planets and Space*, 67(1), 79, doi:10.1186/s40623-015-  
599 0228-9.
- 600 Thomsen, M. F., M. G. Henderson, and V. K. Jordanova (2013), Statistical properties of  
601 the surface-charging environment at geosynchronous orbit, *Space Weather*, 11(5), 237–  
602 244, doi:10.1002/swe.20049.
- 603 Thorne, R. M. (2010), Radiation belt dynamics: The importance of wave-particle interac-  
604 tions, *Geophysical Research Letters*, 37(22), doi:10.1029/2010GL044990.
- 605 Toffoletto, F., S. Sazykin, R. Spiro, and R. Wolf (2003), Inner magnetospheric model-  
606 ing with the Rice Convection Model, *Space Science Reviews*, 107(1-2), 175–196, doi:  
607 10.1023/A:1025532008047.
- 608 Tsyganenko, N. A. (1989), A magnetospheric magnetic field model with a warped tail cur-  
609 rent sheet, *Planetary and Space Science*, 37(1), 5–20, doi:10.1016/0032-0633(89)90066-  
610 4.
- 611 Tsyganenko, N. A., and T. Mukai (2003), Tail plasma sheet models derived from geo-  
612 tail particle data, *Journal of Geophysical Research: Space Physics*, 108(A3), doi:  
613 10.1029/2002JA009707.
- 614 Tsyganenko, N. A., and M. I. Sitnov (2005), Modeling the dynamics of the inner mag-  
615 netosphere during strong geomagnetic storms, *Journal of Geophysical Research: Space*  
616 *Physics*, 110(A3), doi:10.1029/2004JA010798.
- 617 Volland, H. (1973), A semiempirical model of large-scale magnetospheric electric fields,  
618 *Journal of Geophysical Research*, 78(1), 171–180, doi:10.1029/JA078i001p00171.
- 619 Walker, R. J., and M. G. Kivelson (1975), Energization of electrons at synchronous or-  
620 bit by substorm-associated cross-magnetosphere electric fields, *Journal of Geophysical*  
621 *Research*, 80(16), 2074–2082, doi:10.1029/JA080i016p02074.
- 622 Weimer, D. R. (2005), Improved ionospheric electrodynamic models and application  
623 to calculating joule heating rates, *Journal of Geophysical Research: Space Physics*,  
624 110(A5), doi:10.1029/2004JA010884.

625 Zhao, H., X. Li, D. N. Baker, S. G. Claudepierre, J. F. Fennell, J. B. Blake, B. A.  
626 Larsen, R. M. Skoug, H. O. Funsten, R. H. W. Friedel, et al. (2016), Ring current  
627 electron dynamics during geomagnetic storms based on the van allen probes mea-  
628 surements, *Journal of Geophysical Research: Space Physics*, *121*(4), 3333–3346, doi:  
629 10.1002/2016JA022358.

630 Zhelavskaya, I. S., Y. Y. Shprits, and M. Spasojević (2017), Empirical modeling of the  
631 plasmasphere dynamics using neural networks, *Journal of Geophysical Research: Space*  
632 *Physics*, *122*(11), doi:10.1002/2017JA024406.

633 **Figure 1.** (a-c) Van Allen Probe-B observations of electron PSD for  $\mu = 0.1, 2.3,$  and  $9.9$  MeV/G and  $K =$   
 634  $0.3 \text{ G}^{1/2} R_E$  during 17 March 2013 storm. (d) The Kp (green) and SYM-H (red) indices.

635 **Figure 2.** Energies and pitch angles corresponding to different values of the first adiabatic invariant  $\mu$ . The  
 636 second invariant  $K = 0.3 \text{ G}^{1/2} R_E$  is constant. The energies and pitch angles are calculated using dipole field.

637 **Figure 3.** Comparison of the Van Allen Probe-B PSD (left column) with the VERB-4D code results (right  
 638 column) for  $\mu = 0.1, 2.3,$  and  $9.9$  MeV/G and  $K = 0.3 \text{ G}^{1/2} R_E$ . The figure represents an in-situ comparison,  
 639 made at the location of the spacecraft. The mean boundary flux is used.

640 **Figure 4.** Comparison between Van Allen Probe-B data (dashed lines) with the VERB-4D code results  
 641 (solid lines) for  $\mu = 0.1$  MeV/G (a-c),  $2.3$  MeV/G (d-f), and  $9.9$  MeV/G (g-i). Columns correspond to satellite  
 642 passes started at 09:00, 13:30, and 18:00 UT on 17 March (from left to right). The dark-grey regions are lim-  
 643 ited by 25th and 75th percentiles of the outer radial boundary conditions. The light-grey regions are limited  
 644 by 5th and 95th percentiles.

645 **Figure 5.** Comparison of the Van Allen Probe-B PSD (left column) with the VERB-4D code results (right  
 646 column) for  $\mu = 0.1, 2.3,$  and  $9.9$  MeV/G and  $K = 0.3 \text{ G}^{1/2} R_E$  **when radial diffusion is not included in the**  
 647 **simulation.** The mean boundary flux is used.

648 **Figure 6.** Comparison between Van Allen Probe-B data (dashed lines) with the VERB-4D code results  
649 (solid lines) for  $\mu = 0.1$  MeV/G (a-c), 2.3 MeV/G (d-f), and 9.9 MeV/G (g-i) **when SAPS model is included**  
650 **in the simulation.** Columns correspond to satellite passes started at 09:00, 13:30, and 18:00 UT on 17 March  
651 (from left to right). The dark-grey regions are limited by 25th and 75th percentiles of the outer radial bound-  
652 ary conditions. The light-grey regions are limited by 5th and 95th percentiles.

Figure 1.

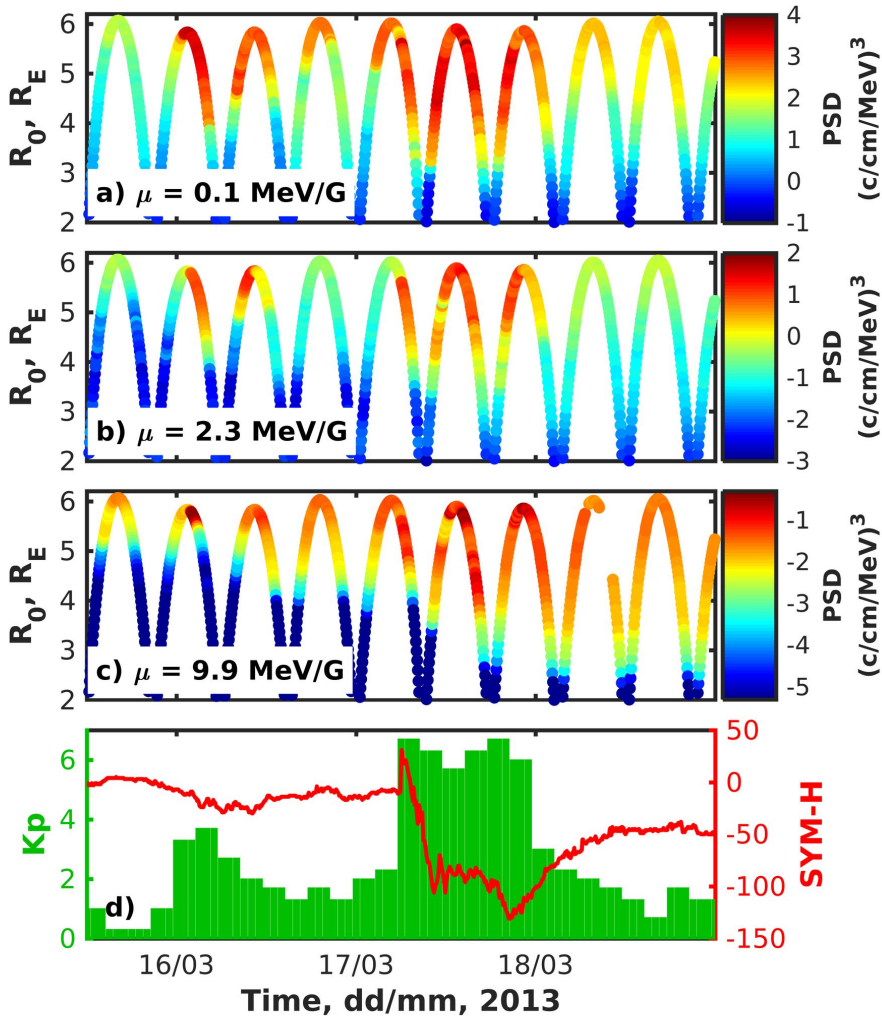


Figure 2.

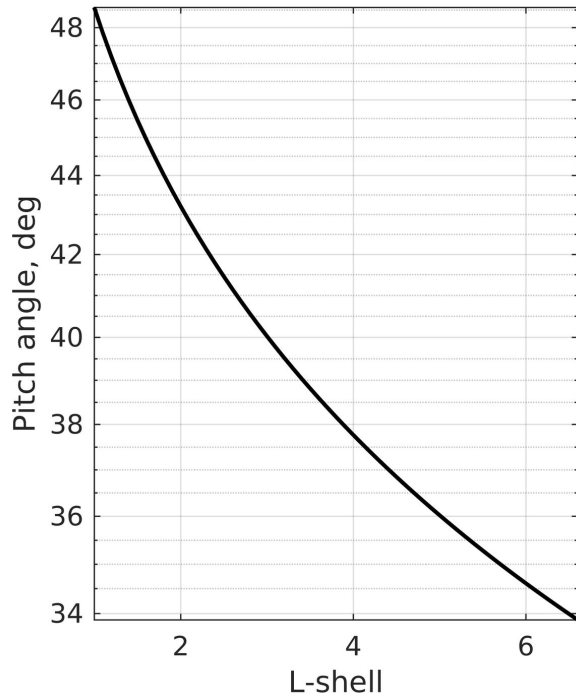
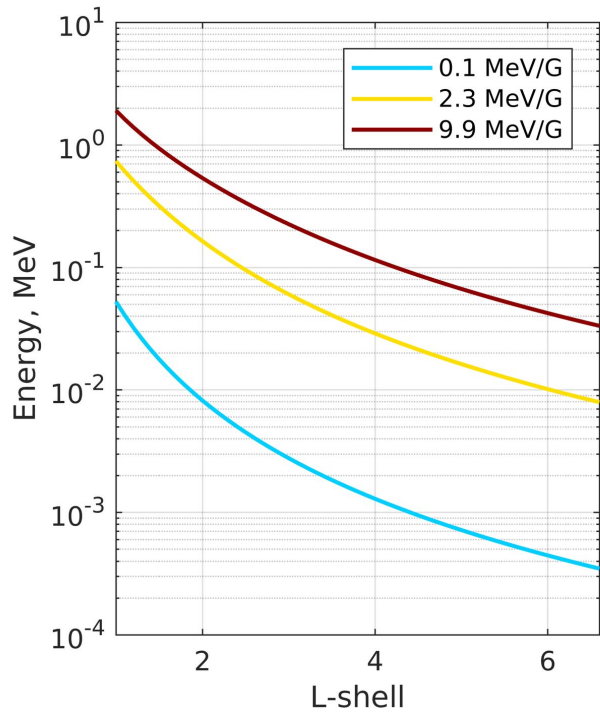
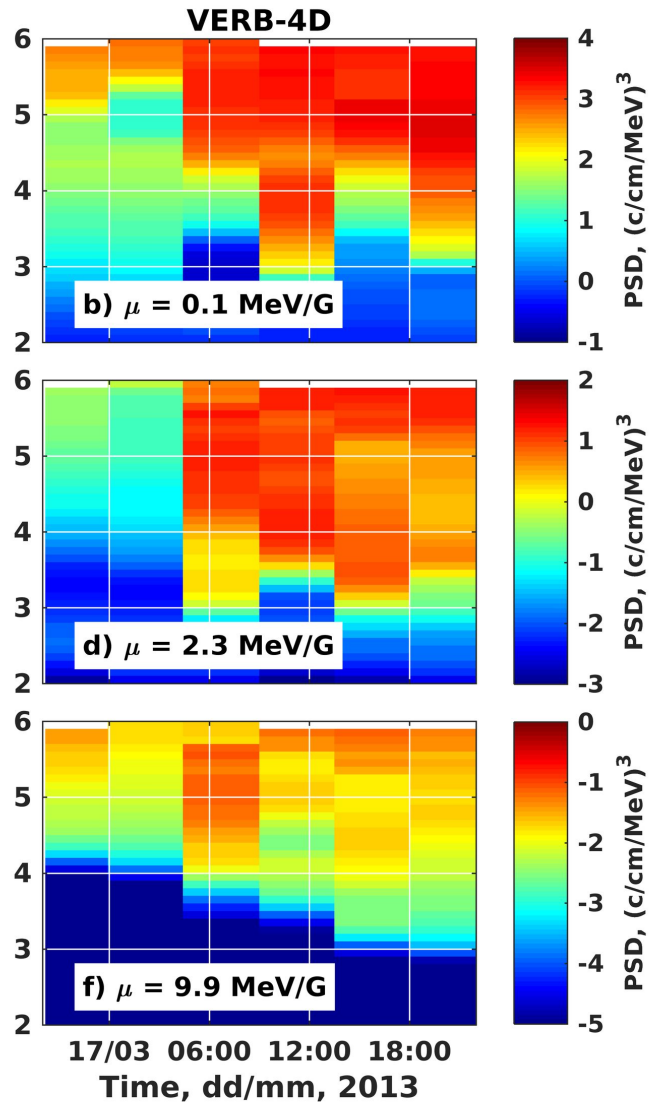
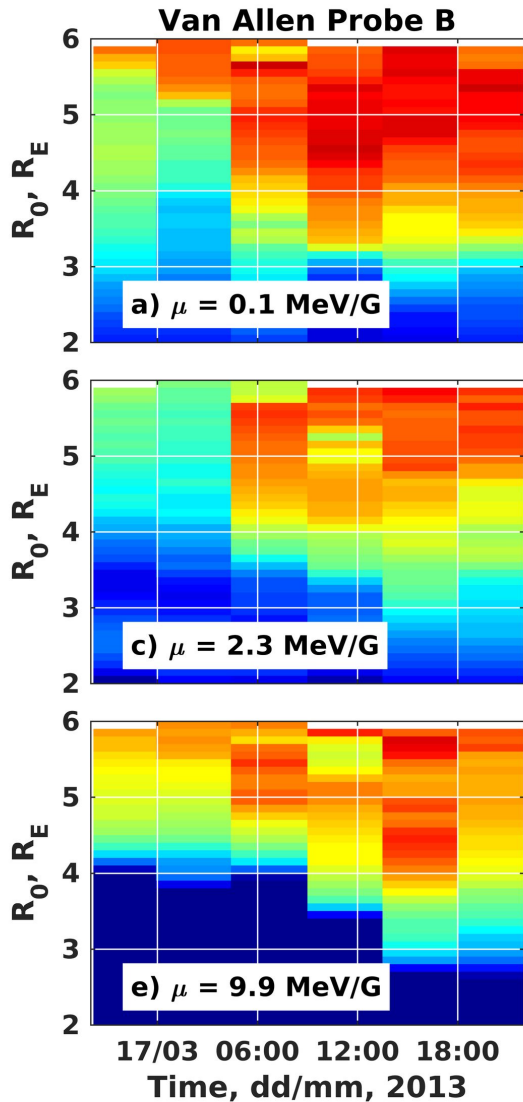
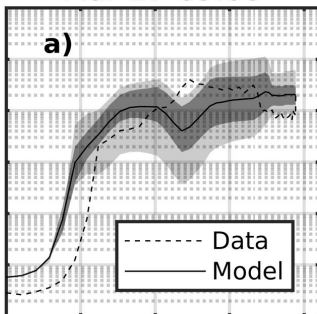


Figure 3.

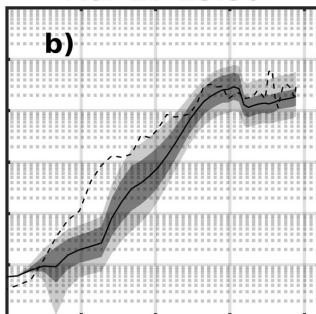


**Figure 4.**

Mar-17-09:00



Mar-17-13:30



Mar-17-18:00

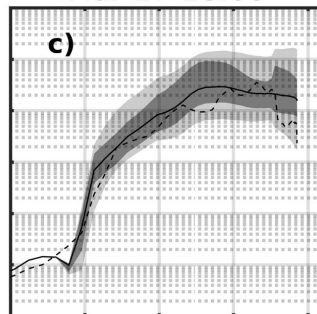
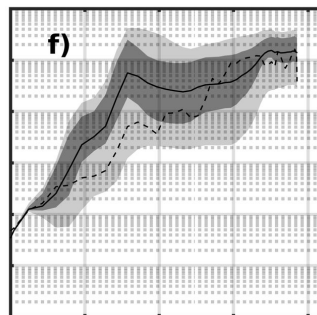
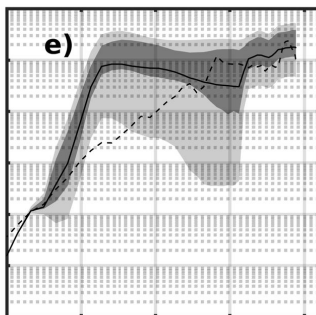
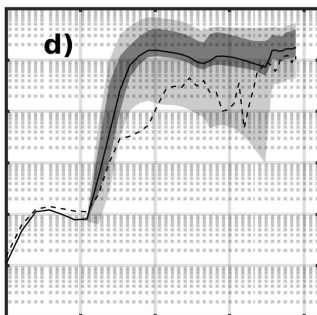
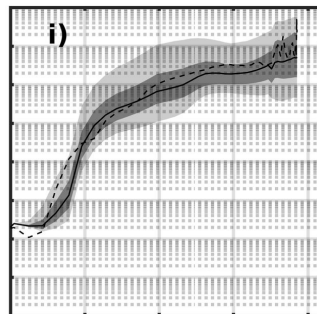
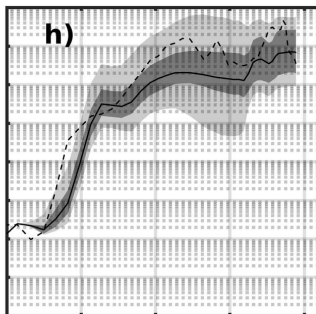
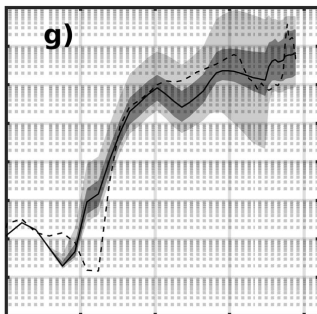
PSD, (c/MeV/cm)<sup>3</sup>PSD, (c/MeV/cm)<sup>3</sup>PSD, (c/MeV/cm)<sup>3</sup>2 3 4 5 6  
 $R_0, R_E$ 2 3 4 5 6  
 $R_0, R_E$ 2 3 4 5 6  
 $R_0, R_E$

Figure 5.

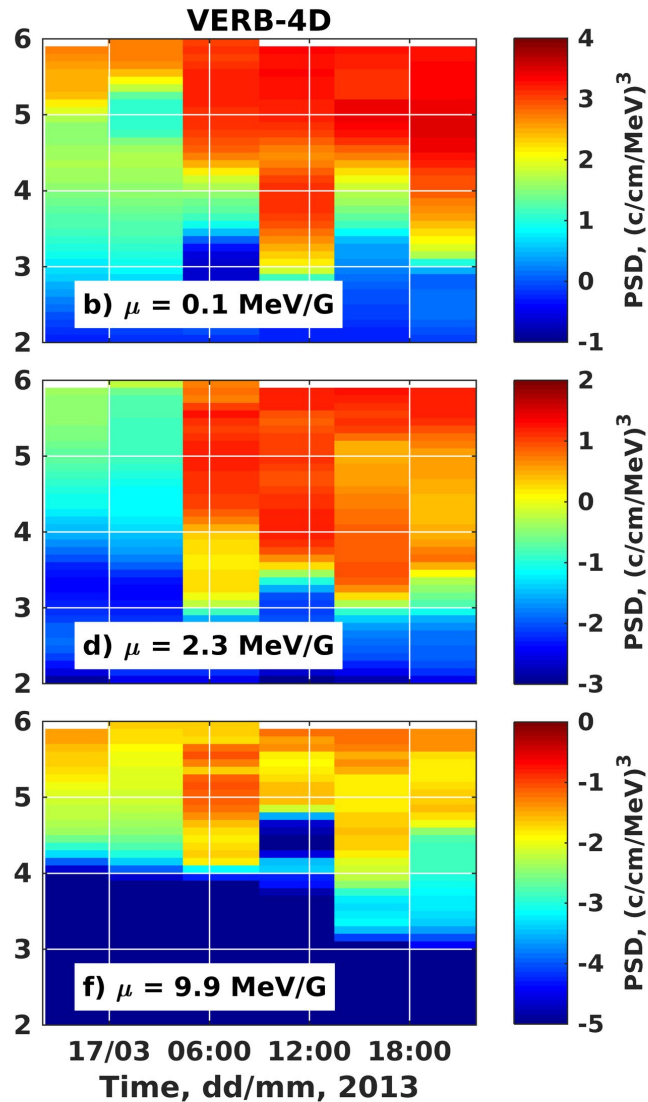
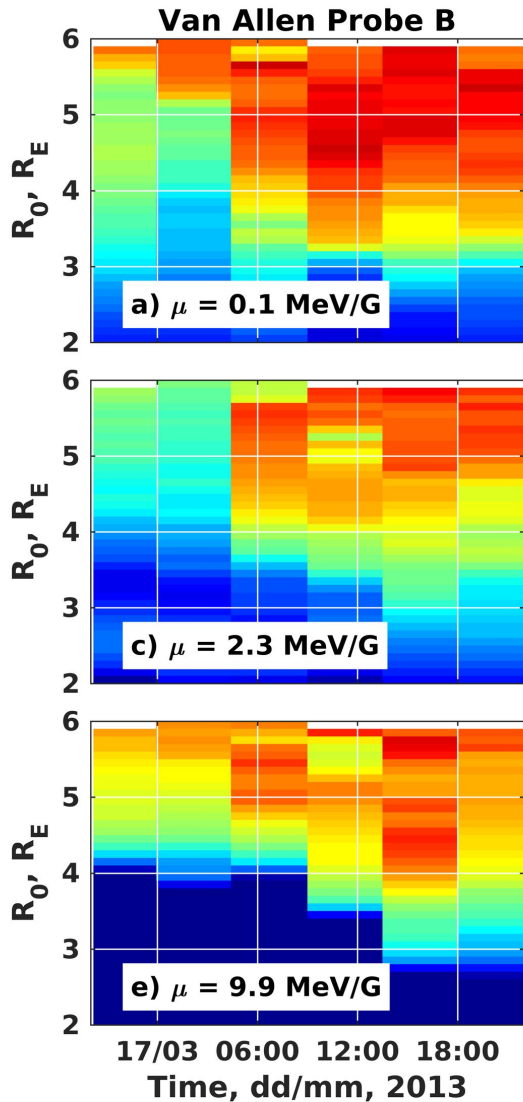
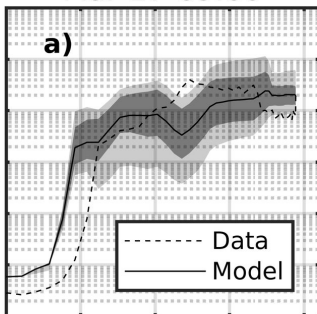
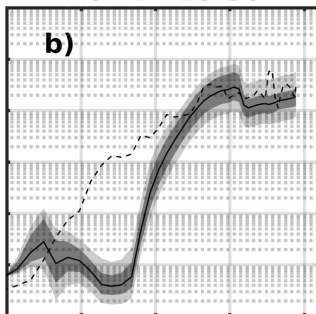


Figure 6.

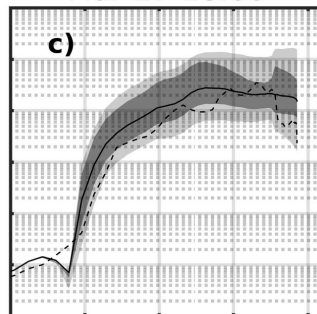
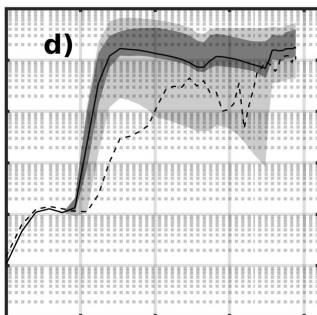
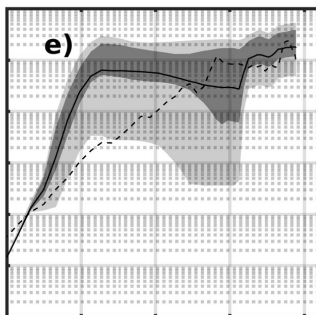
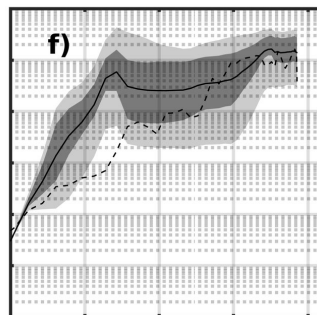
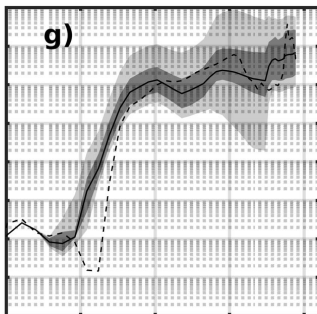
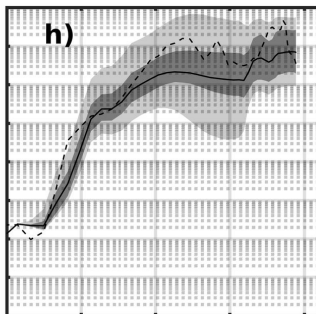
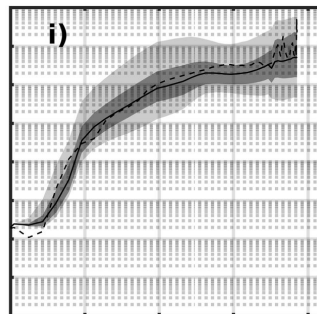
Mar-17-09:00



Mar-17-13:30



Mar-17-18:00

PSD, (c/MeV/cm)<sup>3</sup>**d)** $\mu = 2.3 \text{ MeV/G}$ **e)****f)**PSD, (c/MeV/cm)<sup>3</sup>**g)** $\mu = 9.9 \text{ MeV/G}$ **h)****i)**PSD, (c/MeV/cm)<sup>3</sup>2 3 4 5 6  
 $R_0, R_E$ 2 3 4 5 6  
 $R_0, R_E$ 2 3 4 5 6  
 $R_0, R_E$